Available online at www.sciencedirect.com
ScienceDirect
Trans. Nonferrous Met. Soc. China 24(2014) 3257−3264
Transactions of Nonferrous Metals Society of China
www.tnmsc.cn

Warm bending mechanism of extrados and intrados of large diameter thin-walled CP-Ti tubes

Xiao-li ZHANG, He YANG, Heng LI, Zhi-yong ZHANG, Long LI

State Key Laboratory of Solidification Processing, School of Materials Science and Engineering, Northwestern Polytechnical University, Xi'an 710072, China

Received 12 October 2013; accepted 10 February 2014

Abstract: In order to develop the warming bending technology of the large diameter thin-walled (LDTW) commercial pure titanium alloy CP-Ti tubes, the warm bending mechanism of the extrados and intrados of LDTW CP-Ti tubes was researched. By EBSD analysis and Vickers hardness test, the changes of microstructure and strength of the tubes at different bending temperatures of 293, 423 and 573 K, were analyzed. The results show: 1) The extrados of the bent tube deforms mainly by slip, along with few twinning, and the preferred orientation is similar to that of the initial tube; the intrados of the bent tube experiences compression deformation mainly by $\{10\bar{1}2\}$ tensile twinning, and the twinning makes the preferred orientation of wall materials change sharply. 2) The Vickers hardness values of both the extrados and intrados of the samples after bending increase greatly; the Vickers hardness values of the intrados are much higher than those of the extrados, and Vickers hardness values of the RD−TD planes are always higher than those of the RD−LD planes, which are related to the different deformation mechanisms.

Key words: large diameter thin-walled CP-Ti bent tube; warm bending; texture; twinning; deformation mechanism

1 Introduction

Large diameter thin-walled (LDTW) commercial pure titanium bent tubes, due to their high specific strength and excellent corrosion resistance, are the key components of the pneumatic systems in commercial airplane. To satisfy the airplane for the need of space reduction, the bent tube components with small bending radius R/D (R/D<2 where R is the bending radius and D is the tube outer diameter) are always encountered, which requires large ductility of CP-Ti tube. However, when bending at room temperature, they exhibit strong anisotropy [1], large deformation resistance and low plasticity [2], which make the precise forming difficult. Since the deformation resistance of pure titanium tube may decrease and can get better elongation at elevated temperatures [3], the warm bending may be an effective way to form the LDTW CP-Ti bent tubes. It is important to study the mechanism of the warm bending progress, which is the premise of the precision forming of large diameter thin-walled commercial pure titanium tubes.

Up to now, some researches have been done on the bending process and mechanical performances of CP-Ti. ZHOU et al [4] simulated the hot-push forming technology on TA2 titanium ring pipe by ANSYS, and analyzed the deformation behavior of the extrados and intrados of the tubes during forming process. The Xi'an Aircraft Company (XAC) group [5] experimentally studied the warm bending process of titanium alloy tubes and concluded that at an appropriate heating temperature to the titanium alloy tube, heating was done by electric element and using thermocouple for temperature control. ZHANG et al [6,7] experimentally studied the bending behaviors of LDTW CP-Ti tube in rotary drawing bending at room temperature and further studied the quasi-static tensile behaviors of CP-Ti at elevated temperatures, which are the key factors that influence the warm bending behaviors of tube. WU et al [8,9] experimentally studied the warm bending progress of AM30 magnesium tubes, and found the deformation mechanism of different parts of AM30 magnesium bent tubes. However, the deformation mechanism of LDTW CP-Ti tube under warming bending was less reported.

Foundation item: Projects (50905144, 51275415) supported by the National Natural Science Foundation of China; Project supported by the Program for New Century Excellent Talents in University, China; Project (B08040) supported by the Program of Introducing Talents of Discipline to Universities, China ("111" Project)

Corresponding author: He YANG; Tel/Fax: +86-29-88495632; E-mail: yanghe@nwpu.edu.cn

DOI: 10.1016/S1003-6326(14)63465-8

For titanium alloy with HCP structure, the *c*/*a* value (1.587) is below the ideal one of 1.633. Due to only four independent slip systems in titanium, it is insufficient to adapt to a consecutive plastic strain. Following the von Mises criterion, at least five independent slip systems are needed to accommodate the plastic deformation [10]. In addition to slip, deformation twinning plays an important role in guaranteeing an arbitrary plastic flow of polycrystals at all temperatures. CHUN et al [11] and XU et al [12] experimentally studied the effect of twinning on microstructure and texture evolutions of commercial pure titanium (CP-Ti) during cold rolling and dynamic plastic forming process respectively. SALEM et al [13] studied work hardening effect of twinning on high pure alpha titanium during the simple compression, the plane strain compression and simple shear, and obtained the relationship between the twinning volume fraction and the work hardening rate. HUANG [14] studied the influence of temperature and strain rate on the deformation twinning of polycrystalline titanium by tensile experiments, and found that deformation twinning is dependent on both temperature and strain rate. However, the microstructure evolution and twinning mechanism of CP-Ti tube bent under warming condition need further clarification.

In the present study, we focus on the microstructure evolution and strength change of LDTW CP-Ti tube after warm bending process. By taking LDTW CP-Ti tube of *d*76.2 mm×*t*1.07 mm (*d*/*t*=71.2) as the objective, the specimens for suitable EBSD and Vickers hardness test were designed, and a set of EBSD and Vickers hardness tests was carried out at the temperatures of 293, 423 and 573 K. In terms of the texture evolution, grain-boundary misorientation distribution and Vickers hardness change, the deformation mechanisms during warm bending progress were finally discussed.

2 Experimental

2.1 Materials

The as-received LDTW CP-Ti tube was welded CP-Ti tube in sizes of *d*76.2 mm×*t*1.07 mm following the standard of SAE AMS4941E. As the welded zone was relatively small and it could be placed at the part with small plastic deformation such as the neutral position of tube bending, the effects of the welded zone on the mechanical properties of the LDTW CP-Ti tube could be neglected.

2.2 Procedure

The tubes were warmly bent by a "W27YPC–159" hydraulic bending machine with heating device. The bending angle was 90°, the bending velocity was 1 (°)/s, the bending radius was 2*d* (152.4 mm), and the bending temperatures were 293, 423 and 573 K, respectively. All bent tubes were air cooled to room temperature after bending. Figure 1 shows the schematic diagram of the warm bending progress.

EBSD tests and Vickers hardness tests were chosen to get the microstructure evolution and strength change of the bent tubes. Figure 2 shows the schematic diagram of the sampling location and shape of samples. For the direction, RD refers to tube radial direction, TD refers to hoop direction and LD refers to length direction. As shown in Fig. 2, the samples were cut from the largest deformation regions at the extrados and intrados of the

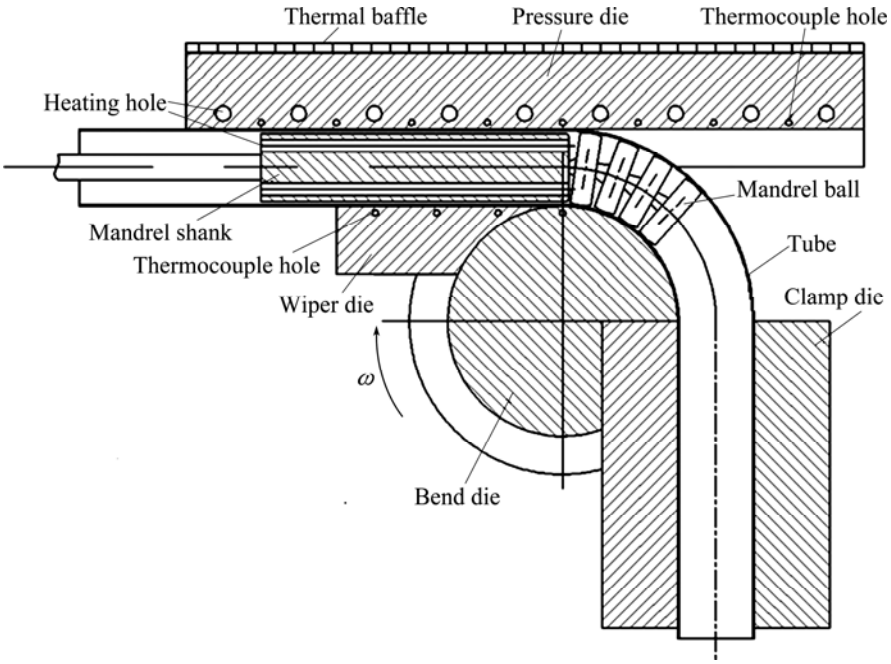

Fig. 1 Schematic diagram of warm bending progress

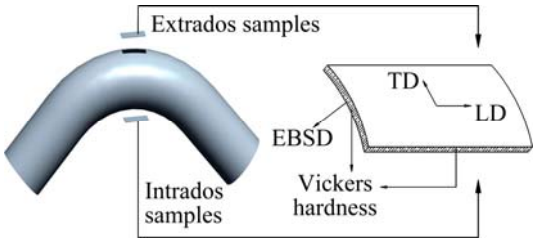

Fig. 2 Schematic diagram showing sampling location and shape of sample

bent tube, respectively. The sample dimensions were 10 mm×10 mm (RD×TD).

After mechanical polishing and chemical corrosion, the Vickers hardness tests were done on the RD−TD and RD−LD surfaces of the samples by HXP−1000TM/LCD micro hardness tester.

To EBSD samples, after mechanical polishing, the electro-polishing was conducted in a solution consisting of 6 mL perchloric acid and 94 mL glacial acetic acid at 30 V and 293 K. The EBSD tests were done on the RD−TD surfaces of the samples with a MIRA3 XMU scanning electron microscope. The data were acquired and processed with the HKL Channel 5 software to get useful maps. The misorientations below 2° are not considered since the deformation can cause orientation uncertainty and orientation noise, possibly leading to blurring of the grain boundaries.

3 Results and discussion

3.1 Texture evolution

By the changes of the EBSD maps and pole figures, the texture evolution was discussed. Figure 3 shows the EBSD map of the as-received material. For the color code, the red for (0001), the green for $(01\bar{1}0)$ and the blue for $(12\bar{3}0)$, give the crystallographic directions of each grain pointing in the direction of LD. As can be seen, the as-received material contains equiaxed grains with an average grain size of 20 μm. And the red and orange dominate the image, which indicates that the *c*-axis of most grains was parallel to the direction of LD. This is verified by the direct pole figure of (0001) shown in Fig. 3(b), which shows a bimodal distribution perpendicular to RD−TD plane. The maximum intensity of 8.92 was found at the locations tilted 45° from LD toward RD, and the second maximum tilted 30° from LD toward RD. As the deformation temperatures were below the transformation temperature (1157 K), and the possible influence of *β*-phase on the deformation behavior can be eliminated.

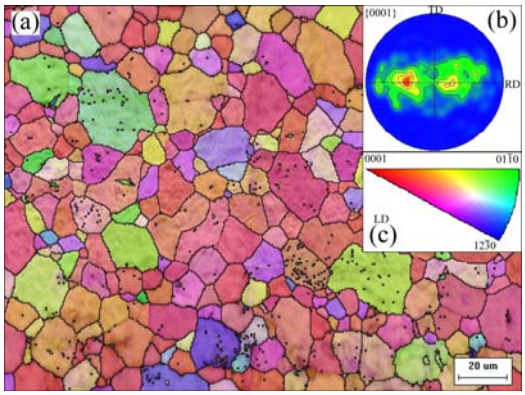

Fig. 3 EBSD map (a) for RD−TD plane of as-received material, (0001) pole figure (b) and Ti-hexagonal IPF coloring inverse pole figure (c)

Figure 4 shows the pole figures of samples under different forming conditions. Preferred orientations of different samples are not consistent. As shown in Figs. 4(a) and (b), after bending at 293 K, the preferred orientation of the extrados sample is still a bimodal texture similar to the original material, while the preferred orientation of the intrados sample of the tube is titled a small angle in the direction TD to RD and perpendicular to the RD−LD plane. Figures 4(c) and (d) show that, after the deformation at 423 K, the preferred orientation of the extrados is also similar to the original material, while the texture of the intrados is similar to that in the case of 293 K, and the maximum intensity can be found in the direction of TD. As shown in Figs. 4(e) and (f), after bending at 573 K, the texture of extrados is similar to the original material, while the maximum intensity of preferred orientation of the intrados is not like the two cases above, presenting a random distribution tendency.

Figure 5 shows the EBSD maps of the extrados and intrados samples bent at 423 K. The grains in Figs. 5(a) and (c) are colored according to a standard color code presented as an inverse pole figure in LD direction and the black lines represent for high angle grain boundaries (HABs). It is obvious that deformation resulted in a development of heterogeneous microstructure. Figure 5(a) shows that some grains were elongated along the direction of LD, and few twinning can be found at the extrados. The color of most of the grains is red, just like the initial material, which indicates that the texture of the extrados of the bent tube under tension did not change much. Figure 5(c) shows that most of the grains are compressed along LD, and the green and blue colors dominate the image indicating the dramatically texture changing. The fragmentation of most grains was caused by twinning. In order to identify the twinning systems activated during warm bending deformation, the misorientation angle and rotation axis of each twin relative to the parent (matrix) orientation were determined from EBSD data. Figures 5(b) and (d) mark the twinning within the grains of the extrados and

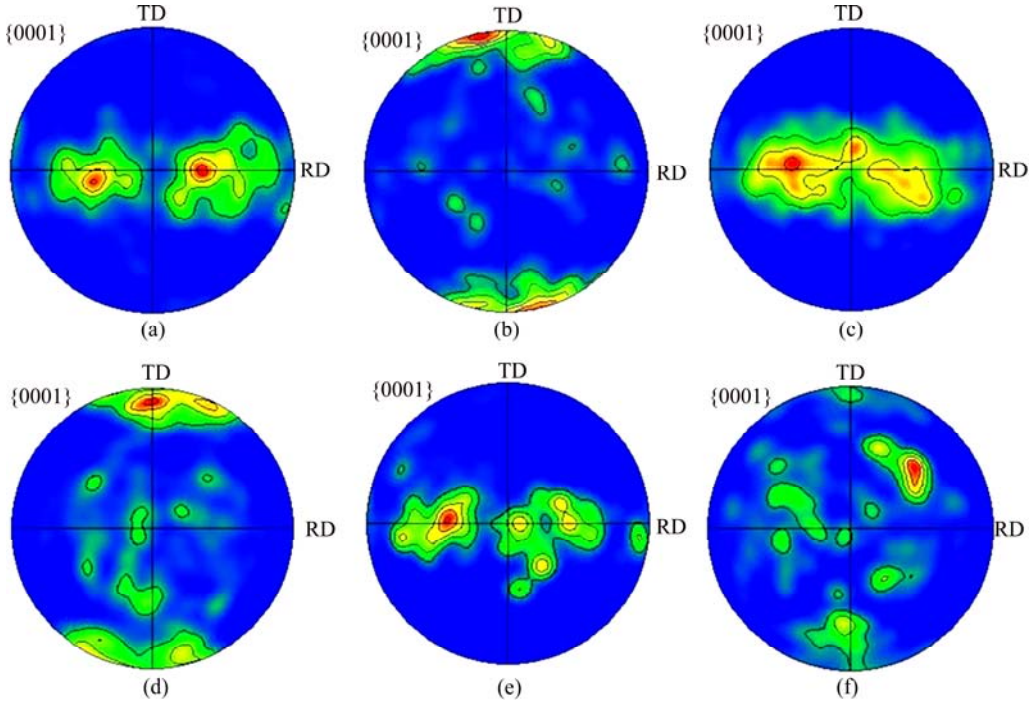

Fig. 4 Pole figures of different samples: (a) 293 K, extrados; (b) 293 K, intrados; (c) 423 K, extrados; (d) 423 K, intrados; (e) 573 K, extrados; (f) 573 K, intrados

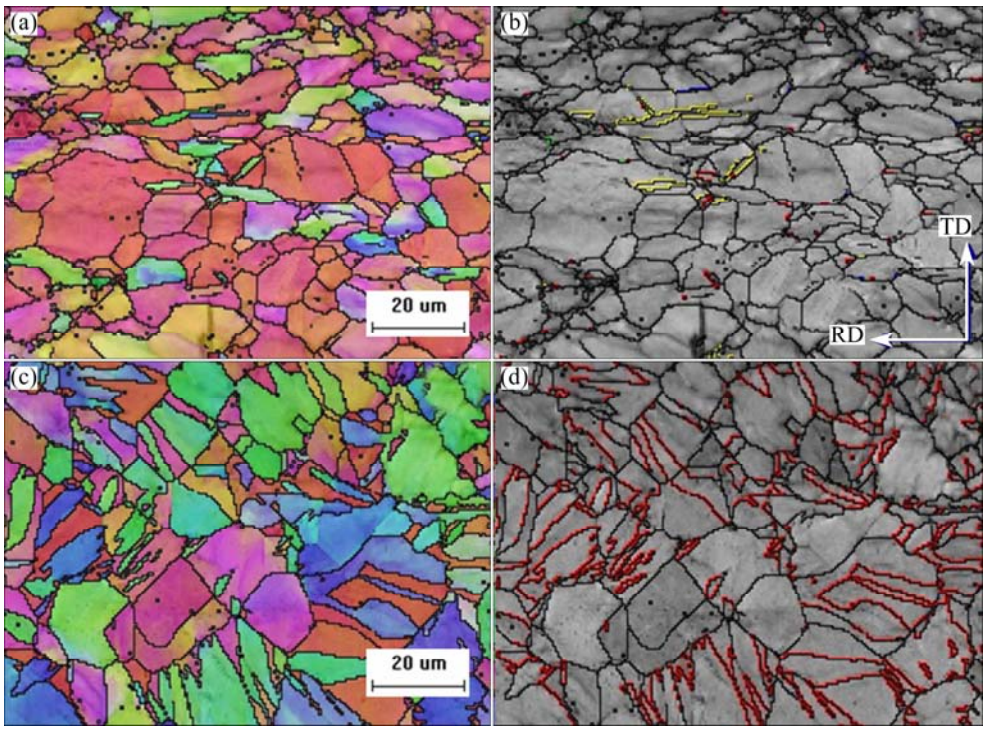

Fig. 5 EBSD maps of extrados and intrados samples bent at 423 K: (a), (b) Extrados; (c), (d) Intrados

intrados of the bent tube with different colors, respectively, viz., blue for $\{11\bar{2}4\}$ twinning, yellow for $\{11\bar{2}2\}$ twinning, red for $\{10\bar{1}2\}$ twinning and green for $\{11\bar{2}1\}$ twinning. Figure 5(b) shows that a few amount of yellow-marked twinning occurred, i.e. $\{11\bar{2}2\}$ twinning, and the other three types of twinning are rare. Figure 5(d) shows that a large amount of red-marked twinning happened, i.e. $\{10\bar{1}2\}$ twinning, and other three types of twinning are rare.

The EBSD analysis results of other samples are summarized in Table 1, which shows the volume fraction of all kinds of twinnings and the low angle grain

Table 1 Volume fraction of twinning and amount of LABs under different conditions (volume fraction, %)

Twinning	293 K		423 K		573 K	
	Extrados	Intrados	Extrados	Intrados	Extrados	Intrados
$\{11\bar{2}4\}$ blue	0.242	0.182	0.062	0.056	0.096	0.120
$\{11\bar{2}2\}$ yellow	1.35	0.682	0.352	0.014	0.377	0.537
$\{10\bar{1}2\}$ red	1.59	5.110	0.439	7.540	2.960	6.970
$\{11\bar{2}1\}$ green	0.0266	0.145	0.057	0.044	0.019	0.071
Total	3.2086	6.119	0.910	7.654	3.451	7.698
LABs	51.566	26.009	37.021	24.497	43.003	30.486

boundaries (LABs) under different forming conditions. The data show that after the deformation, the extrados and intrados of the bent tube show completely different deformation mechanisms. The twinning volume fraction at the extrados of the bent tube is quite small, while at the intrados a large number of $\{10\bar{1}2\}$ twinnings can be found. And after warm bending, the amount of low angle grain boundary is sharply raised, which indicates the occurring of the dislocation slip in the tube wall [15], and at the same temperature, the number of LABs of the extrados is always higher than that of the intrados.

3.2 Plastic deformation mechanism

During the warm bending process, the plastic deformation mechanisms of the extrados and the intrados are entirely different. At the extrados, slip is the dominate mechanism of plastic deformation. However, for CP-Ti with HCP structure, there are only two independent basal slip systems, far fewer than the five independent systems necessary for general plastic deformation of polycrystals. Therefore, the basal slip system, nonbasal slip system and a small amount of deformation twinning work together to accommodate the plastic deformation [16,17]. For the intrados of samples under compression, the twinning deformation is very active.

From Fig. 3 it is known that the *c*-axis of most grains is parallel to the direction of LD. During bending, the extrados of the tube is under tension, and the tensile direction is parallel to LD; with the deformation happening, the *c*-axis of most grains is still parallel to the tensile direction (Figs. 4(a), (c), (e)), which is a suitable condition for the occurring of the $\{11\bar{2}2\}$ compressive twinning. While the critical shear stress that the $\{11\bar{2}2\}$ compressive twinning needs is too high, so there is few twinning happening at the extrados. While the intrados of the tube is under compression, the compressive direction is parallel to LD. From Figs. 4(b), (d), (f), it is found that the *c*-axes of most grains have approximate 90° rotating after bending, which makes the compressive direction and *c*-axes of most grains in a vertical relationship. The vertical relationship is a favorable condition for the happening for $\{10\bar{1}2\}$ tensile twinning. $\{10\bar{1}2\}$ tensile twinning for its low shear and only simple atoms moving, can easily occur. In bending deformation, similar to other HCP metals, the deformation of CP-Ti begins with slip, but since the number of active slip systems is less than that of BCC or FCC metals, the deformation twinning begins to play a vital role. A large amount of $\{10\bar{1}2\}$ tensile twinning is found at the intrados of the tube wall, which is consistent with the result by XU et al [12] that $\{10\bar{1}2\}$ tension twinning always appears at the beginning of the deformation. And a small amount of $\{11\bar{2}2\}$ compressive twinning can also be found, which is consistent with the result by PATON and BACKOFEN [18] that the $\{11\bar{2}2\}$ twinning can only occur under 300 °C. The other two types of twinnings are very few, and almost can be neglected. Twinning can also change the crystal orientation to make it easy to slip. The proliferation of low angle grain boundaries can be concluded that in order to accommodate the plastic deformation, slip is also essential.

Figure 6 shows that the misorientation distribution varies with the deformation conditions. The plastic deformation mechanism of warm bending can also be concluded from the misorientation distribution. It can be seen that the misorientation exhibits peaks at 30°, 65° and 87°. And the peak at 30° can be frequently found, and according to the result reported by VALLE et al [19], the peak at 30° indicates that two adjacent grains belong to the basal fiber texture. As it is common for deformed HCP metals, such as CP-Ti and Mg alloys, to have a strong basal texture, the 30° peak is expected. After bending at 293, 423 and 573 K, compared with the extrados of the bent tube wall, the misorientation distribution of the intrados of the bent tube showed two peaks: one at about 65° and another at about 87° except basal fiber texture about 30°. These two peaks represent the $\{11\bar{2}2\}$ compressive twinning and $\{10\bar{1}2\}$ tensile twinning respectively. The peak at 87° is much sharper, which indicates that $\{10\bar{1}2\}$ tensile twinning is the

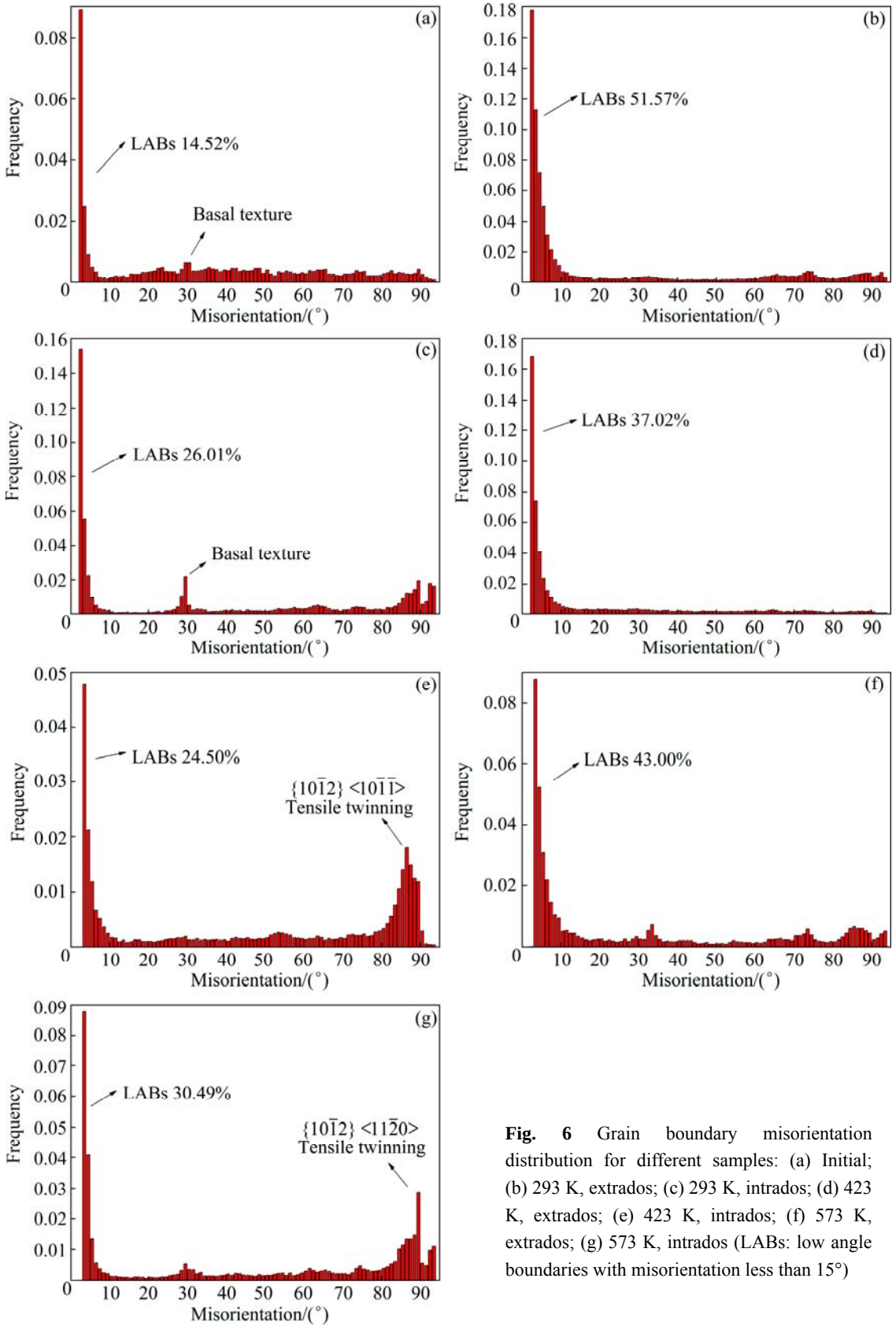

Fig. 6 Grain boundary misorientation distribution for different samples: (a) Initial; (b) 293 K, extrados; (c) 293 K, intrados; (d) 423 K, extrados; (e) 423 K, intrados; (f) 573 K, extrados; (g) 573 K, intrados (LABs: low angle boundaries with misorientation less than 15°)

main mechanism of plastic deformation at the intrados during warm bending. The number of high-angle grain boundaries also has a dramatic increase due to the twinning, while the low angle grain boundary does not reduce. This phenomenon indicates that, although twinning is the main mechanism during the bending, the

slip also plays an important role in accommodating the plastic deformation. After bending at 293, 423 and 573 K, the low angle grain boundaries of the misorientation distribution of the extrados tubes under tension show a dramatic increase while its high angle grain boundaries are not radically changed, which is consistent with the result mentioned above that the plastic deformation mechanism at the extrados of the tube is mainly composed of slip and twinning is very weak.

Texture evolution is related to the main plastic deformation mechanism. 1) At the extrados of the tube wall under tension during bending, the preferred orientation is similar to that of the original material, not very big change. This is due to the fact that the main plastic deformation mechanism is slip, which will not produce much change to the preferred orientation of polycrystal. 2) At the intrados of the tube wall under compression, texture changes violently. This is because a large number of twinnings are found at the intrados of the tube wall.

3.3 Vickers hardness

Figure 7 shows the Vickers hardness values of the RD−LD planes and RD−TD planes of both the intrados and extrados of the bent tubes. After bending at different temperatures, the Vickers hardness values of the RD−LD planes and RD−TD planes of both the extrados and intrados of the samples increase greatly, and peak at 293 K. The Vickers hardness values of the intrados of the tubes are always higher than those of the extrados, and the Vickers hardness values of RD−TD planes are always higher than those of RD−TD planes.

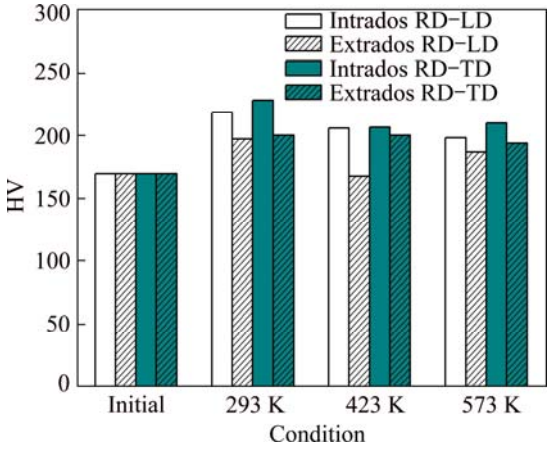

Fig. 7 Vickers hardness values of samples under different deformation conditions

The changes of the Vickers hardness values are closely associated with the microstructure evolution. 1) Compared with the original materials, the Vickers hardness values are greatly improved after bending, which is consistent with the proliferation of low angle grain boundaries. This is because a large number of low angle grain boundaries and a few deformation twinnings are found at the extrados of the tube wall and the intrados of the tube wall generate a large number of twinnings after deformation. The proliferation of low angle grain boundaries produces work hardening of the material, which results in an increase of Vickers hardness. Twinning can make grains refine so that the Vickers hardness value is improved. 2) The Vickers hardness values of the intrados samples under compression are relatively higher than those of the extrados samples under tension, which indicates that the enhancing effect in Vickers hardness of twinning is far greater than that of low angle grain boundaries. 3) The Vickers hardness values of the RD−TD planes are always higher than those of the RD−LD planes, which is related to both the preferred orientation changes and the microstructure evolution.

4 Conclusions

1) After bending at different temperatures, the plastic deformation mechanisms of the extrados and intrados of CP-Ti titanium tubes are different. The plastic deformation mechanism of the extrados under tension is mainly slip and twinning is weak. The intrados under compression are mainly deformed by twinning and added with slip, and main type of twinning is $\{10\bar{1}2\}$ tensile twinning.

2) After bending at different temperatures, the texture of the extrados samples under tension is similar to that of the initial tubes. The intrados of the bent tube experienced compression and deformed mainly by $\{10\bar{1}2\}$ tensile twinning, and approximate 90° rotating happened for the texture of the intrados under compression after bending at 293 and 423 K, while the preferred orientation presents a random distribution tendency at 573 K.

3) After bending at different temperatures, the Vickers hardness values of the RD−LD plane and RD−TD plane of both the intrados and the extrados of the bent tubes increase greatly, and peak at 293 K. The Vickers hardness values of the intrados are much higher than those of the extrados, and the Vickers hardness values of the RD−TD planes are always higher than those of the RD-LD planes, which are related to the different deformation mechanism.

References

[1] WANG Gang, ZHANG Kai-feng, WU De-zhong, WANG Jun-zhi, YU Yan-dong. Superplastic forming of bellows expansion joints made of titanium alloys [J]. Journal of Materials Processing Technology, 2006, 178(1−3): 24−28.

[2] JIANG Zhi-qiang, YANG He, ZHAN Mei, XU Xu-dong, LI Guang-jun. State-of-the-arts and prospectives of manufacturing and application of titanium alloy tube in aviation industry [J]. Journal of Plasticity Engineering, 2009, 16(4): 44−50. (in Chinese)
[3] LIU Jaan-ming, CHOU Sheh-shou. Study on the microstructure and formability of commercially pure titanium in two-temperature deep drawing [J]. Journal of Materials Processing Technology, 1999, 95(1−3): 65−70.
[4] ZHOU Wei, ZHOU Lian, YU Zhen-tao. Finite element numerical simulation of hot-push forming technology on TA2 titanium ring pipe [J]. Rare Metal Material and Engineering, 2005, 34(10): 1585−1587. (in Chinese)
[5] MAO Jun-feng, ZHANG Ye. Bending forming technology of aerospace titanium tube [J]. Intelligence and Information, 2000(2): 49−52. (in Chinese)
[6] ZHANG Zhi-yong, YANG He, LI Heng, REN Ning, WANG Dan. Quasi-static tensile behavior and constitutive modeling of large diameter thin-walled commercial pure titanium tube [J]. Materials Science and Engineering A, 2013, 569: 96−105.
[7] ZHANG Zhi-yong, YANG He, LI Heng, REN Ning, TIAN Yu-li. Bending behaviors of large diameter thin-walled CP-Ti tube in rotary draw bending [J]. Progress in Natural Science: Materials International, 2011, 21(5): 401−412.
[8] WU Wen-yu, JIN Li, DONG Jie, PENG Li-ming, YAO Shou-shan. Bendability mechanisms in AM30 alloy tube using a rotary draw bender [J]. Materials and Manufacturing Processes, 2010, 25(12): 1359−1364.
[9] WU Wen-yun, ZHANG Ping, ZENG Xiao-qin, JIN Li, YAO Shou-shan, LUO A A. Bendability of the wrought magnesium alloy AM30 tubes using a rotary draw bender [J]. Materials Science and Engineering A, 2008, 486(1−2): 596−601.
[10] TAYLOR G I. Plastic strain in metels [J]. Journal of the Institute of Metals, 1938, 62: 307−324.
[11] CHUN Y B, YU S H, SEMIATIN S L, HWANG S K. Effect of deformation twinning on microstructure and texture evolution during cold rolling of CP-titanium [J] .Materials Science and Engineering A, 2005, 398(1−2): 209−219.
[12] XU Feng, ZHANG Xi-yan, NI Hai-taoi, CHENG You-ming, ZHU Yu-tao, LIU Qing. Effect of twinning on microstructure and texture evolutions of pure Ti during dynamic plastic deformation [J]. Materials Science and Engineering A, 2013, 564: 22−33.
[13] SALEM A A, KALIDINDI S R, DOHERTY R D. Strain hardening of titanium: Role of deformation twinning [J]. Acta Materialia, 2003, 51(14): 4225−4237.
[14] HUANG Wen, WANG Yang, LI Zi-ran, XIA Yuan-ming. Influences of temperature and strain rate on deformation twinning of polycrystalline titanium [J]. The Chinese Journal of Nonferrous Metals, 2008, 18(8): 1440−1445. (in Chinese)
[15] TAN J C, TAN M J. Dynamic continuous recrystallization characteristics in two stage deformation of Mg−3Al−1Zn alloysheet [J]. Materials Science and Engineering A, 2003, 339: 124−132.
[16] CHRISTIAN J W, MAHAJAN S. Deformation twinning [J]. Progress in Material Science, 1995, 39(1−2): 1−157.
[17] PARTRIDGE P G. The crystallography and deformation modes of hexagonal close-packed metals [J]. International Materials Reviews, 1967, 12(1): 169−194.
[18] PATON N E, BACKOFEN W A. Plastic deformation of titanium at elevated temperatures [J]. Metall Trans, 1970, 1(10): 2839−2847.
[19] DEL VALLE J A, PEREZ-PRADO M T, RUANO O A. Deformation mechanisms responsible for the high ductility in a Mg AZ31 alloy analyzed by electron backscattered diffraction [J]. Metallurgical and Materials Transactions A, 2005, 36(6): 1427−1438.

大口径薄壁纯钛管数控热弯内外侧的塑性变形机制

张晓丽，杨 合，李 恒，张志勇，李 龙

西北工业大学 材料学院，国家凝固重点实验室，西安 710072

摘 要：为了发展大直径薄壁纯钛管数控加热弯曲技术，实验研究了大口径薄壁 CP-3 管材在不同温度下数控弯曲后的内外侧塑性变形机制。通过 EBSD 分析和维氏显微硬度测试方法，对数控弯曲温度 293、423 和 573 K 下弯管件试样弯曲外侧受拉区域以及弯曲内侧受压区域进行显微组织变化和维氏硬度分析。结果表明：1) 在不同温度下数控弯曲变形后，弯管外侧塑性变形机制主要为滑移，孪生变形微弱，择优取向类似于初始管材的；弯管内侧塑性变形机制主要以 $\{10\bar{1}2\}$ 孪晶为主，滑移为辅助机制，且孪晶使管壁材料择优取向产生剧烈转变。2) 维氏硬度的变化与塑性变形机制及织构有关。弯曲变形后，管材试样内外侧轴向与周向的维氏硬度值均显著得到提高，且管材试样内侧的维氏硬度值要明显高于外侧的，周向的维氏硬度值高于轴向的。

关键词：大口径薄壁商业纯钛管；加热弯曲；织构；孪晶；塑性变形机制

(Edited by Hua YANG)